Growth kinetics and modeling of selective molecular beam epitaxial growth of GaAs ridge quantum wires on pre-patterned nonplanar substrates

Taketomo Sato,[a] Isao Tamai, and Hideki Hasegawa
Research Center for Integrated Quantum Electronics (RCIQE) and Graduate School of Electronics and Information Engineering, Hokkaido University, Kita-Ku, Sapporo 060-8628, Japan

(Received 18 January 2004; accepted 23 March 2004; published 20 August 2004)

The growth kinetics involved in the selective molecular beam epitaxial growth of GaAs ridge QWRs is investigated in detail experimentally and an attempt is made to model the growth theoretically. For this purpose, detailed experiments were carried out on the growth of ⟨110⟩-oriented AlGaAs–GaAs ridge quantum wires on mesa-patterned (001) GaAs substrates. A phenomenological modeling was done based on the continuum approximation including parameters such as group III adatom lifetime, diffusion constant and migration length. Computer simulation using the resultant model well reproduces the experimentally observed growth features such as the cross-sectional structure of the ridge wire and its temporal evolution, its temperature dependence and evolution of facet boundary planes. The simple phenomenological model developed here seems to be very useful for design and precise control of the growth process. © *2004 American Vacuum Society.*
[DOI: 10.1116/1.1773841]

I. INTRODUCTION

Recently, intensive research efforts have been made on semiconductor quantum devices such as single electron transistors and quantum wire transistors. For the realization of large scale integrated circuits using such devices, it is necessary to form networks of high quality and highly uniform quantum structure in a size- and position-controlled fashion.

Selective molecular beam epitaxy (MBE)/metal organic vapor phase epitaxy (MOVPE) technique of III–V semiconductors on pre-patterned substrates is one of the most promising technique for the formation of position—and size-controlled arrays of quantum wires (QWRs) and quantum dots (QDs).[1–4] Recently, we have reported that ⟨110⟩-oriented QWRs and related network structures can be successfully formed for both InP-[5] and GaAs-based materials[6–8] on (001) patterned substrates by a selective MBE growth. However, growth on nonplanar substrates usually involves various high-index facets simultaneously which complicates growth kinetics.[9] For precise control of wire cross section and feature sizes, a quantitative modeling of the growth process based on proper understanding of the underlying growth mechanism is a key issue.

Until recently, a large number of efforts on numerical modeling of the crystal growth have been reported not only on epitaxial growth on planar substrates[10–13] but also on growth on nonplanar substrates.[14–18] For the latter, use of diffusion equations under the continuum approximation with phenomenological macroscopic parameters such as diffusion constants, migration length and incorporation rates, as initiated by a pioneering work by Ohtsuka and Miyazawa,[14] has become a standard approach, being capable of reproducing evolution of complex growth profiles of micron-meter sized structures qualitatively or semiquantitatively. However, since the previous works emphasized mathematical aspects of modeling, comparison with experiments were poor, and it is not clear whether suitable modeling based on such an approach can quantitatively reproduce the experimentally observed evolution of cross-sectional features of nanometer-sized quantum structures in such way that it can be utilized for design and control of growth of nanostructures.

The purpose of this paper is to experimentally investigate and theoretically model the growth kinetics involved in the selective MBE growth of GaAs ridge QWRs in a view of their size- and position-control. For this purpose, detailed experiments were carried out on the growth of ⟨110⟩-oriented GaAs wires on mesa-patterned substrates, and a phenomenological modeling based on the continuum approximation was attempted. Theoretical calculation using the resultant model well reproduced the experimentally observed growth features such as the cross-sectional structure of the ridge wire and its temporal evolution, its temperature dependence and evolution of facet boundary planes. The simple phenomenological model developed in this study seems to be very useful for design and precise control of the growth process of nanostructures.

II. EXPERIMENTAL STUDY OF GROWTH KINETICS

A. Growth method and cross-sectional features

Our method of wire formation by selective MBE growth is schematically shown in Fig. 1(a) for the case of the ⟨110⟩-oriented GaAs ridge quantum wire grown on a (001) patterned substrate. Since growth of this wire is very well behaved and highly reproducible,[6,7,19] the experimental study and modeling in this study were concentrated on the growth of this wire.

Referring to Fig. 1(a), the wire was grown by the following sequence. As a template for the selective growth, a ⟨110⟩-oriented mesa pattern was first formed on semi-insulating GaAs (001) substrates by a standard lithography and wet etching process. The resultant mesa-structures have a (001)

[a]Author to whom correspondence should be addressed; electronic mail: taketomo@rciqe.hokudai.ac.jp

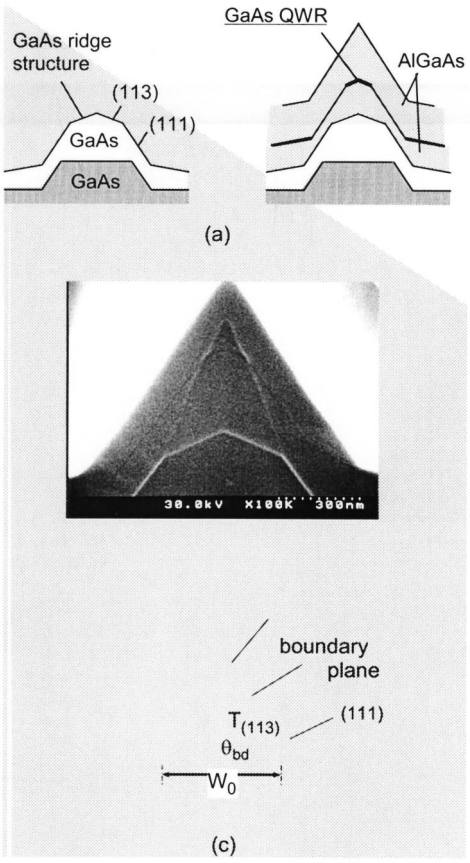

FIG. 1. (a) Growth process, (b) cross-sectional SEM image, and (c) its schematic representation of the $\langle \bar{1}10 \rangle$-oriented GaAs ridge nanowire.

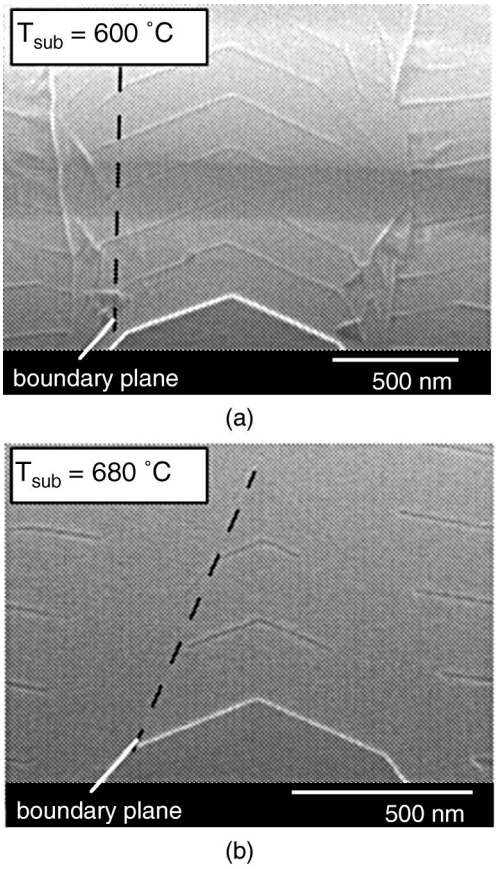

FIG. 2. Cross-sectional SEM images of samples after repeated growth at (a) $T_{sub}=600\,^{\circ}\mathrm{C}$ and (b) $T_{sub}=680\,^{\circ}\mathrm{C}$.

top facet and two (111) side facets. After surface treatments in the atmosphere, thermal cleaning under arsenic pressure was applied in the MBE chamber just before the growth. Then, a GaAs buffer layer was grown on the patterned substrate. This led to the formation of GaAs ridge structures defined by two (113) facets which newly appeared during the growth. Then, materials for the growth of $Al_{0.3}Ga_{0.7}As$–GaAs–$Al_{0.3}Ga_{0.7}As$ layers were supplied onto the GaAs (113) buffer ridge, and this resulted in the formation of embedded wires. The growth rate of GaAs and AlGaAs layers were kept to be 700 and 1000 nm/h, respectively, in terms of the values for growth on a planar reference substrate placed next to the patterned substrate.

The cross section of the wire after cleavage along the $(\bar{1}10)$ plane was completely featureless under SEM observation. However, a complex features became visible after stain etching by an alkali solution. A resultant cross-sectional scanning electron micrograph (SEM) image is shown in Fig. 1(b), and its schematic representation is given in Fig. 1(c). It is clearly seen that an arrow-head shaped GaAs nanowire bounded by AlGaAs (113) facets with a reduced size is selectively formed above the top (113) facets of the GaAs ridge structure with the initial ridge width, W_o. Presence of thin GaAs quantum well along (111) side facets can also be recognized. In addition to these, presence of white lines in Fig. 1(b) which are indicated by dashed lines in Fig. 1(c) is obvious. By previous repeated growth experiments,[7,19] these lines have been identified to correspond to planar boundaries between the region grown on the (111) facets and that grown on the (113) facets within the AlGaAs barrier layers, and they were termed as the ''facet boundary planes.'' It is obvious that these planes play important roles in determining the width and height of the wire. For the sake of the discussion in this paper, let us define the boundary angle, θ_{bd}, as the angle formed by the boundary plane with respect to the (001) plane.

At first, one might think that these boundary planes themselves correspond to particular crystalline facets that are activated during the growth. However, detailed measurements have shown that it is not a case.[7,19] In fact, they were found to depend strongly on the growth temperature, T_{sub}. The cross-sectional SEM images of the test structures grown at $T_{sub}=600\,^{\circ}\mathrm{C}$ and $680\,^{\circ}\mathrm{C}$, are shown in Figs. 2(a) and 2(b), respectively. In each test structure, growth of a thin GaAs wire was repeated by the repeated supply of AlGaAs–GaAs–AlGaAs materials starting from the bottom GaAs ridge structure. It is seen in both cases that previous growth memory is remarkably kept in spite of the insertion of a GaAs layer, and the boundary angle was kept constant throughout the entire growth. As seen in Figs. 2(a) and 2(b) θ_{bd} was large at low growth temperatures, and the wire width did not change so much throughout the repeated wire

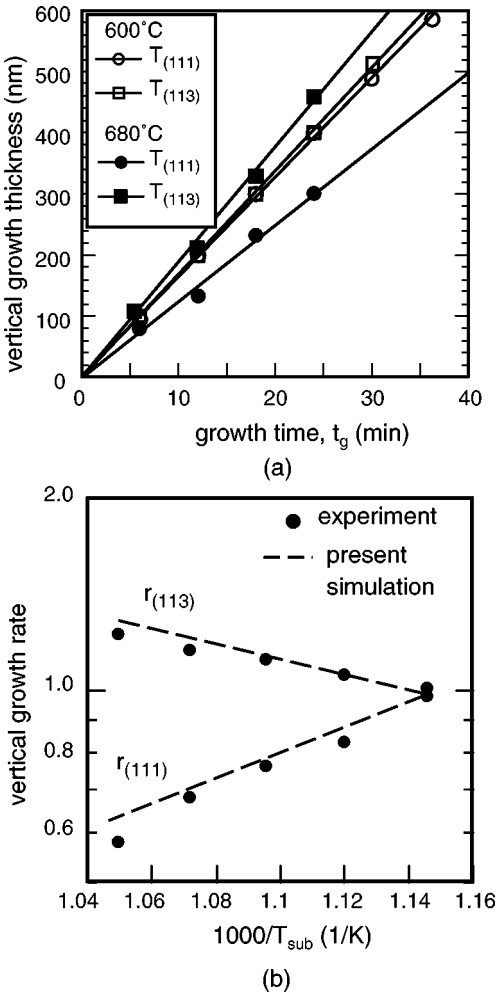

FIG. 3. (a) Vertical growth thickness on (111) and (113) facets vs growth time, t_g, and (b) the vertical growth rate ratio on (111) facets and (113) facets plotted as a function of $1000/T_{sub}$.

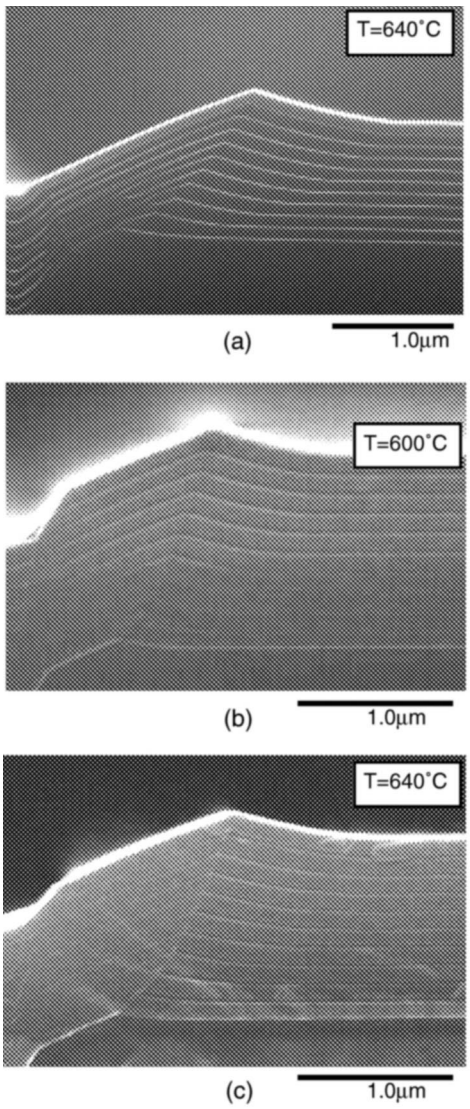

FIG. 4. Cross-sectional SEM images of the sample after repeated growth of (a) GaAs(95 nm)–AlAs(5 nm) layers at 640 °C, (b) AlGaAs(100 nm)/GaAs(10 nm) at 600 °C and (b) AlGaAs(100 nm)–GaAs(10 nm) at 640 °C.

growth. On the other hand, at the higher growth temperatures, θ_{bd} became smaller, and the wire width decreased rapidly with the growth time, t_g.

B. Growth rates on different facets

Change of the wire cross section with time can be represented quantitatively in terms of the changes with time of the vertical thicknesses, $T_{(113)}$ and $T_{(111)}$ defined in Fig. 1(c) where the former is for the region grown on the (113) ridge and the latter for the region grown on the (111) side facets. Examples of the measured values of $T_{(113)}$ and $T_{(111)}$ are plotted in Fig. 3(a) versus the growth time, t_g. As seen in Fig. 3(a), they change in proportion to t_g as expected. Then, the vertical growth rates can be defined as $r_{(113)}=\mathrm{d}\,T_{(113)}/\mathrm{d}\,t_g$ and $r_{(111)}=\mathrm{d}\,T_{(111)}/\mathrm{d}\,t_g$, respectively. The measured values of $r_{(113)}$ and $r_{(111)}$ are plotted vs inverse of the substrate temperature T_{sub}(K) during growth in Fig. 3(b). The broken lines in Fig. 3(b) are the results of computer simulation explained later.

Thus, it can be said that, for precisely controlled growth of QWRs, a theoretical understanding and quantitative modeling of evolution of cross-sectional features such as appearance of new facets, change of cross section with time and evolution of boundary planes are necessary.

C. Growth on one-sided mesa pattern

In order further get information on growth kinetics, growth experiments on one-sided mesa step were carried out. The substrate pattern was a GaAs step structure consisting of a (111) side facet and (001) top and bottom facets where the top width is long enough to be able to see the variation of the grown thickness in the lateral direction.

Figure 4(a) shows the cross-sectional SEM image of the sample after the repeated growth of GaAs (95 nm)–AlAs (5 nm) layers at $T_{sub}=640\,^{\circ}\mathrm{C}$ where AlAs layers were used as markers, and thickness values of 95 and 5 nm are those for growth on (001) planar substrates. Similarly, Figs. 4(b) and 4(c) show the results after the repeated growth of

AlGaAs(100 nm)–GaAs(10 nm) layers at two different substrate temperatures of $T_{sub}=600\,^{\circ}\mathrm{C}$ and 640 °C where GaAs layers were used as markers.

As seen in Figs. 4(a)–4(c), growth behavior of GaAs layers AlGaAs layers on the substrate step is very similar, and shows the following two remarkable features. One is the appearance and development of a new (113) facet on the left-hand side of the boundary of (111) and (001) facets, and the other was extended variation of grown thickness on the right-hand side which seems to show exponential decay. The latter is obviously due to the additional flux of adatoms from the neighboring side facet by diffusion.

III. PHENOMENOLOGICAL MODELING OF SELECTIVE GROWTH

A. Basic equations

As a means of quantitative theoretical description of the selective MBE growth, an attempt was made here to model the growth process by using a phenomenological description based on the continuum approximation. The physical situation for growth on a nonplanar substrate is schematically shown in Fig. 5(a). Here, growth of a $\langle\bar{1}10\rangle$-oriented infinitely long GaAs QWR on a mesa stripe pattern formed on (001) substrate is considered, and the problem is treated as a two-dimensional (2D) one. As shown in Fig. 5(a), the z axis and x axis are taken to be in the vertical $\langle 001\rangle$ direction and in the lateral $\langle 110\rangle$ direction, respectively.

The surface density of the group III adatoms, $n(x,t_g)$, at the lateral position, x, and the growth time, t_g satisfies the following equation:

$$\frac{\mathrm{d}n(x,t_g)}{\mathrm{d}t_g}=G\cdot\cos\theta-\frac{n(x,t_g)}{\tau(\theta)}-\frac{\mathrm{d}J(x,t_g)}{\mathrm{d}x}, \tag{1}$$

where G is the incident flux of atoms coming from the source in vacuum, θ is the surface slope angle measured with respect to the x axis, and $\tau(\theta)$ is the lifetime of the group III adatoms until they are incorporated into the surface. Here, it is assumed that neither desorption of group III adatoms nor dissociation of crystal takes place during the crystal growth, and that the growth rate is limited by incorporation of group III adatoms. These assumptions are known to be valid in the standard MBE growth.

The surface flux, $J(x,t_g)$, in Eq. (1) is given by the following Nernst–Einstein relation:

$$J(x,t_g)=-D\frac{n(x,t_g)}{k_BT}\cdot\mathrm{grad}(U), \tag{2}$$

where D is the diffusion coefficient of adatoms on the surface and U is the chemical potential in the growth system. As seen in Eq. (2), the gradients of the chemical potential determine the surface diffusion toward a lower potential. In general, the internal chemical potential, U_{int}, is distinguished from the external chemical potential, U_{ext}, and the total chemical potential, U, in the system is the sum of U_{int} and U_{ext}. They could be represented as follows:

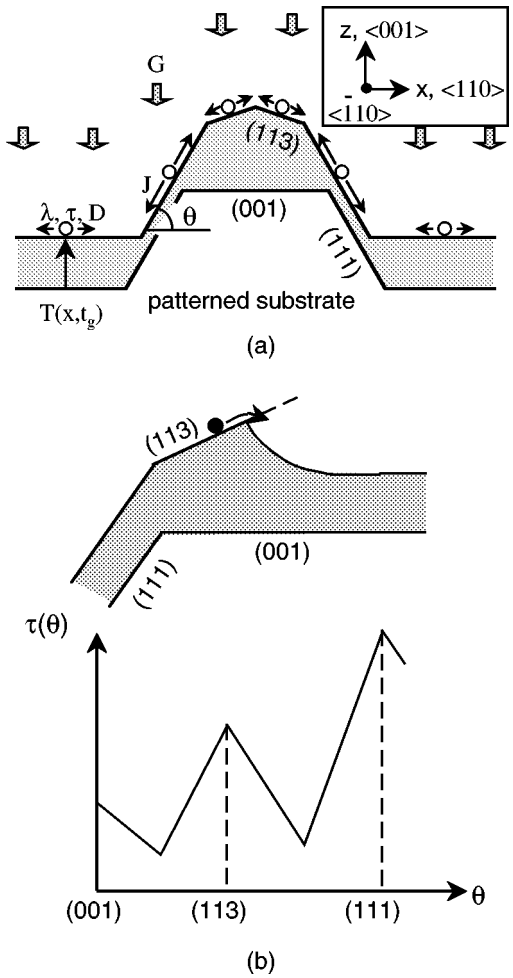

FIG. 5. (a) Model of growth on nonplaner substrates for a theoretical calculation and (b) the schematics of faceting growth with the slope dependent lifetime, $\tau(\theta)$.

$$U_{\mathrm{int}}=k_BT\cdot\log\left(\frac{n(x,t_g)}{n_Q}\right), \tag{3}$$

$$U_{\mathrm{ext}}=U_{\mathrm{strain}}+U_{\mathrm{alloy}}+U_{\mathrm{surface}}. \tag{4}$$

In Eq. (3), the U_{int} for adatoms is represented as the chemical potential of the mobile species in two-dimensional ideal gas, where n_Q is a constant value related to a reference point of the chemical potential. On the other hand, U_{ext} for adatoms is represented by the total sum of the chemical potential due to surface strain, U_{strain}, the entropy of alloy mixing, U_{alloy}, and the surface free energy involving the capillarity effect, U_{surface}. As for the case of GaAs–AlAs alloy semiconductors, the surface strain is almost negligible. Furthermore, the mixing reaction of this system seems to be much smaller than those of the other alloys such as InAs–GaAs and InAs–AlAs. Therefore, it could be assumed that U_{surface} accounts for the most part of the external chemical potential, U_{ext}. Additionally, Ozdemir *et al.*[16] and Biasiol *et al.*[18] included the capillarity effect in their calculation as the main driving factor for surface diffusion of adatoms. Using this, Eq. (4) can be rewritten as follows:

$$U_{\text{ext}} = U_{\text{surface}} = \mu_0 + \frac{\Omega \gamma_s}{r_c}, \tag{5}$$

where μ_0 is the chemical potential of bulk and Ω is the atomic volume. γ_s and r_c are the surface free energy and the radius of curvature, respectively, at the position, x, and the time, t_g. Since the surface free energy term is a slow varying function as compared with the growth curvature, it can be taken to be a constant independent of facet and position as a first approximation. By taking account of the capillarity effect in this way, any further complex treatment of the boundary condition between the neighboring facets is not necessary.

After the calculation of the adatom density, $n(x,t_g)$, the cross-sectional growth profile is obtained by plotting the vertical growth thickness, $T(x,t_g)$, which is represented by the following equation as a function of the lateral position, x, and the growth time, t_g:

$$T(x,t_g) = \int_0^{t_g} \frac{n(x,t)\cdot\Omega}{\tau \cos\theta}. \tag{6}$$

When there are more than one species of group III adatoms as in the case of growth of AlGaAs, Eq. (2) was solved separately for each species, and each contribution was added together in calculating Eq. (6).

B. Method of calculation and values of parameters

The calculation on evolution of the cross-sectional structure of the wire was carried out by numerically solving the differential equation of Eq. (1), starting from the initial mesa pattern consisting of (001) top facet and two (111) side facets and standing on a (001) plane. For this purpose, the wire cross section was divided into a fine mesh structure, and a standard finite difference method was applied.

For the calculation, values of the various parameters were required. It is obvious that, the surface lifetime, $\tau(\theta)$, and the diffusion coefficient, D, of group III adatoms are most important parameters which determine the growth features.

The lifetime of group III adatoms is expected to be more strongly dependent on the step densities of the growing surface rather than the difference of adatom species. Thus, it is assumed here that the surface lifetime of Ga adatom, and that of Al adatom, are the same, but they depend strongly on the surface slope, θ, as indicated as $\tau(\theta)$. The dependence of $\tau(\theta)$ on θ assumed in this study is schematically shown in Fig. 5(b). Since the exact functional dependence of $\tau(\theta)$ is unknown, we employed a piecewise linear form as shown in Fig. 5(b) as a first approximation. On the other hand, a different approach for fitting was used recently by Ohtsuka[15] where the diffusion equation was solved on a terrace with steps to arrive at a functional of $\tau(\theta)$. However, it is not clear how appropriate it is to force the macroscopic diffusion equation to the events of atomic level on the step-terrace structures with the mesoscopic length scale. Thus, we sought for a simplified piecewise linear functional dependence shown in Fig. 5(b) in order to describe gross average behavior of the atomic scale movements near facet boundaries.

In our fitting procedure, $\tau(\theta)$ has local maxima at particular surface slope angles which correspond to (001), (113), and (111) singular facets that appeared in the present wire growth. The values of $\tau(\theta)$ on the characteristic (001), (113), and (111) singular facets are denoted as $\tau_{(001)}$, $\tau_{(113)}$, and $\tau_{(111)}$, and they should be closely related to the vertical growth rates measured in the experiments. However, the relationships between these quantities are not direct ones, since the vertical growth rates are also related to the lateral diffusion of group III adatoms. The value of $\tau(\theta)$ rapidly decreases from these peaks, and this represents the physical situation that step densities are high at such surface slope angles. There, the growth proceeds rapidly so as to modify the slope in such a way that it reaches quickly the slowly growing characteristic facet and stays there as schematically shown in Fig. 5(b). Therefore, we used $\tau_{(001)}$, $\tau_{(113)}$, and $\tau_{(111)}$ as well as the positions and lifetime values of local minima in the piecewise linear portions graph as the fitting parameters in the present modeling. The temperature dependence of $\tau(\theta)$ was ignored, although a weak decrease with temperature in Arrhenius form is expected according to Monte Carlo simulation of GaAs (001) surface by Kangawa *et al.*[13] The reported activation energy is 0.35 eV, and this change the value of τ by a negligibly small factor of 1.4 for the substrate temperature range of 600–680 °C in the present experiment.

As for the diffusion constant, the growth results shown in Fig. 4 should provide information. Namely, Eq. (2) reduces to the following famous equation for the growth on a crystalline facet under an additional supply of group III adatoms by lateral diffusion:[20,21]

$$\Delta T(x) = \Delta T(0)\exp(-x/\lambda), \tag{7a}$$

where $\Delta T(x)$ is increase of grown thickness due to diffusion at the lateral position, x, and λ is the migration length of the group III adatoms on the facet given by

$$\lambda = (D\tau)^{1/2}. \tag{7b}$$

The measured growth thickness increase is plotted in Fig. 6(a) as a function of lateral distance as defined in the inset. The thickness indeed decreased exponentially with the lateral distance increased following by the relation in Eq. (7a). From that, the value of the migration length, λ, was estimated to be 400 nm for growth of GaAs on GaAs at $T_{\text{sub}} = 640$ °C and 90, 370 and 950 nm for growth of AlGaAs on GaAs at the $T_{\text{sub}} = 600$ °C, 640 °C, and 680 °C, respectively. It is well known that migration length of Ga adatoms is much longer than that of Al adatoms. For example, Koshiba *et al.*[22] reported $\lambda(\text{Ga}) = 1000$ nm and $\lambda(\text{Al}) = 40$ nm on (001) GaAs at $T_{\text{sub}} = 610$ °C. Thus, the above results basically corresponds to that of Ga adatoms.

The experimentally obtained diffusion lengths are plotted in Fig. 6(b) as a function of the inverse of the growth temperature, T_{sub}. The data were fitted by the assuming an Arrhenius temperature dependence of $\lambda = \lambda_0 \times \exp(-E_d/2\text{kT})$, and the activation energy of adatom diffusion, E_d, of 4.3 eV was obtained. The present E_d value is consistent with a value of 4.0 eV reported by Van Hove

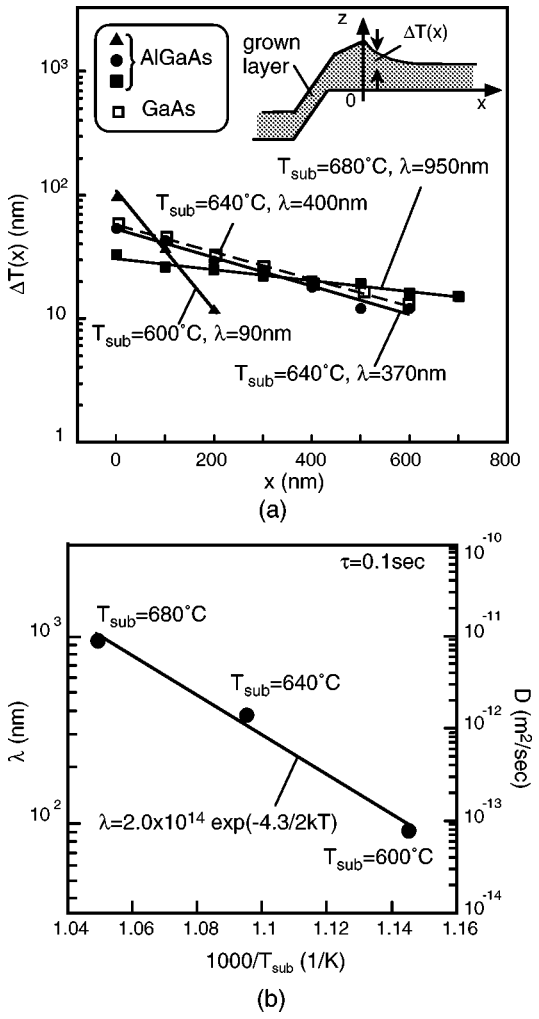

FIG. 6. (a) Variation of growth thickness measured as a function of the lateral position and (b) the experimentally determined diffusion length vs $1000/T_{\mathrm{sub}}$.

et al.,[23] but it is much larger than 0.7 eV reported by Hata *et al.*[20] and 2.8 eV reported by Ohta *et al.*[24] The difference of E_d values seen in those experiments seems to be due to the difference of arsenic pressures during the growth, because the diffusion length of adatoms becomes larger under lower arsenic pressure, as reported by Shen *et al.*[25] The V/III flux ratio used in this study was 30, which was much higher than the V/III ratio of 1 used in the experiment by Ohta *et al.*[24] On the other hand, Van Hove *et al.*[23] used V/III ratio of 10. Thus, the present E_d of 4.3 eV seems to represent a value under a high arsenic pressure condition.

Since diffusion profile measurements were not carried out on facets other than (001) facet, we assumed that the value of the diffusion constant, D, was the same on the other facets with the same temperature dependence in the calculation. In order to take account of the migration length difference in Ga and Al atoms, we assumed the value of D for Al atoms is 100 times smaller than that for Ga atoms, i.e., $\lambda(\mathrm{Ga})=10\lambda(\mathrm{Al})$, in the calculation.

As for the other parameters in the basic equations, the surface free energy, γ_s, was taken to be 3 eV, referring the work by Gebauer *et al.*[26] n_Q and μ_0 disappear by taking gradients.

IV. REPRODUCTION OF GROWTH EXPERIMENTS BY MODELING

A. Growth profiles and growth rates

In order to see how well the present modeling can reproduce the experimental results quantitatively, the growth of ridge QWRs was simulated on computer using the computer program which solves Eq. (1) by the finite difference method.

To reproduce the experimentally observed evolution of cross-sectional structures and to obtain good agreement between simulation and experiments as regards the time variation of the cross section, choice of the values of $\tau_{(001)}$, $\tau_{(113)}$, and $\tau_{(111)}$ was found to be extremely important. First of all, relation of $\tau_{(001)}<\tau_{(113)}<\tau_{(111)}$ was essential to reproduce the experimentally observed evolution of the cross-sectional structure of wires including the stage of the GaAs ridge growth. In other words, the whole process can be regarded as a transition from growth on (001) facet to that on (111) facet triggered by presence of a side (111) facet. Thus, appearance of (113) facet is a transition stage due to presence of a local maximum in $\tau(\theta)$.

Although not as important as the maxima, the positions and lifetime values of lifetime local minima were found to be also important in reproducing details of the evolution behavior of the ridge structures. They were found to be closely related to details of the transitional profile shape, its time evolution and their temperature dependence as the growth proceeds to reveal the new singular facet having a larger lifetime. For example, when the local minimum between the (113) and (111) lifetime peaks was chosen to take place either very close to the (113) peak or very close to the (111) peak, the temperature dependence of the ridge evolution almost disappeared as opposed to the experimental findings.

From such observations, efforts were made to reproduce the experimentally observed vertical growth rates quantitatively by choosing a suitable set of values of $\tau_{(001)}$, $\tau_{(113)}$, $\tau_{(111)}$, and the values of slopes connecting them. The optimum functional behavior of $\tau(\theta)$ found under such a piecewise linear approximation is summarized in Fig. 7(a). Namely, the optimum value of $\tau_{(001)}=100$ ms with a relation of $\tau_{(001)}:\tau_{(113)}:\tau_{(111)}=1:2.5:10$ was obtained. The optimal minimum position between (001) and (113) lifetime peaks was 5°, and that between the (113) and (111) facets was 36°.

The values of vertical growth rates obtained under the optimal simulation conditions are shown in Fig. 3(b) by broken lines. They are in excellent agreement with experimental data within a maximum deviation of 5%.

The growth sequence of GaAs buffer layer on $\langle\bar{1}10\rangle$-oriented mesa structures simulated under the optimum values of $\tau_{(001)}, \tau_{(113)}, \tau_{(111)}$ and the diffusion constant explained in the previous section is shown in Fig. 7(b). At the early growth stage, the growth thickness at both edge of (001) top mesa increased due to the surface diffusion of adatoms from the neighboring side (111) facets. After sufficient growth, the

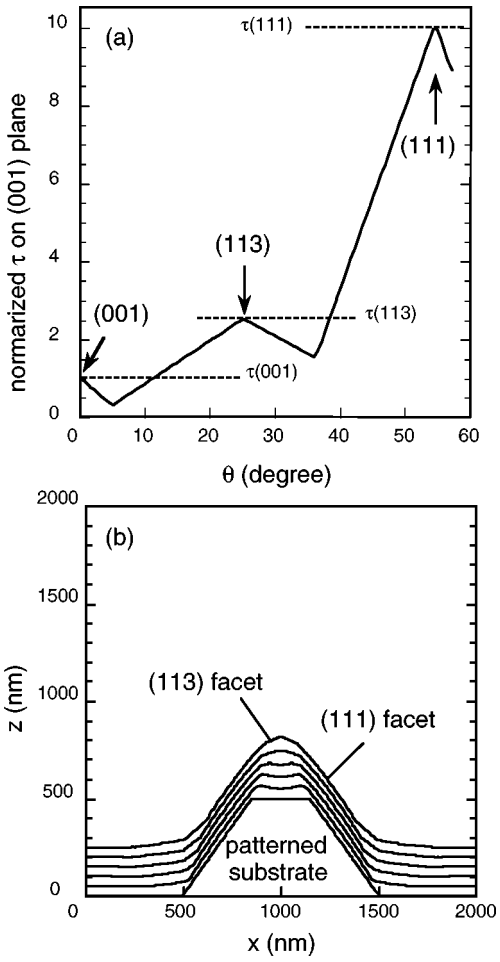

FIG. 7. (a) Optimum piecewise linear graph of $\tau(\theta)$ determined by simulation and (b) the calculated growth sequence of GaAs buffer layer.

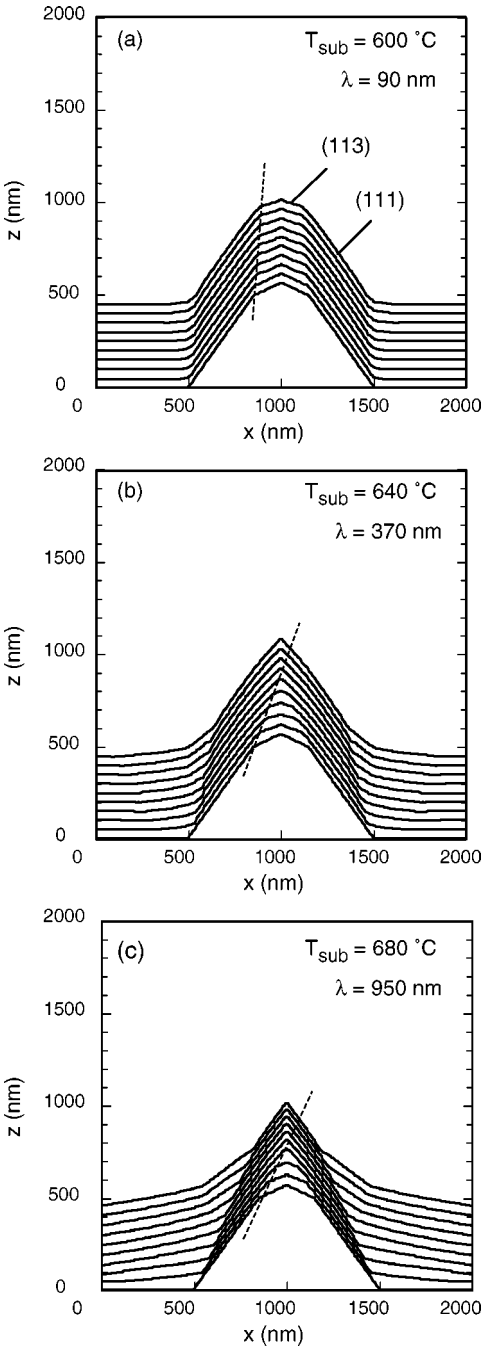

FIG. 8. Calculated growth profiles of the $Al_{0.3}Ga_{0.7}As$ layer on GaAs ridge structures; (a) $T_{sub}=600\,°C$, (b) $T_{sub}=640\,°C$, and (c) $T_{sub}=680\,°C$.

GaAs ridge structure having top (113) facets and side (111) facets were formed on the ⟨110⟩-oriented mesa structure, as seen in Fig. 7(b). The simulation well reproduced the features of experimentally grown GaAs ridge structures.

Figures 8(a)–8(c) show the calculated profile of $Al_{0.3}Ga_{0.7}As$ layers on GaAs ridge structures by changing the T_{sub} of 600 °C, 640 °C, and 680 °C, respectively. As shown in Figs. 8(a)–8(c), the growth profiles of AlGaAs layer were strongly dependent on the growth temperatures. Namely, the widths of top (113) facets of AlGaAs ridge decrease and the ridge shapes become sharp, as T_{sub} was increased. This is because the migration length λ increased from 90 to 950 nm, and adatoms easily moved from the side (111) facets to the top (113) facets or to the bottom (001) plane. Furthermore, the facet boundary planes were clearly shown in the simulation of repeated growth, as indicated by the dashed lines in Figs. 8(a)–8(c). These growth features agree with those observed in the experiment that are shown in Figs. 1(b), 2(a), and 2(b).

In order further to clarify how well our model calculation reproduces the experiment quantitatively, the difference of growth profiles as obtained by subtracting the calculated profile from the experimental one is shown in Fig. 9 for the growth of an AlGaAs ridge structure on the GaAs ridge. Referring to Fig. 1(c), the amount of growth was 300 nm in terms of the vertical thickness $T_{(113)}$ and the initial GaAs ridge width W_0 was 450 nm. The profiles were obtained at 600 °C, 640 °C, and 680 °C. On the ridge top region where a QWR is to be formed, the deviation was found to be very small only within a 5 nm (1.6% of $T_{(113)}$) which is close to the special resolution limit of our SEM observation. Thus, our model calculation well reproduced the growth profile of the important ridge QWR region. However, a slightly larger deviation of about 10 nm (3.3% of $T_{(113)}$) was observed

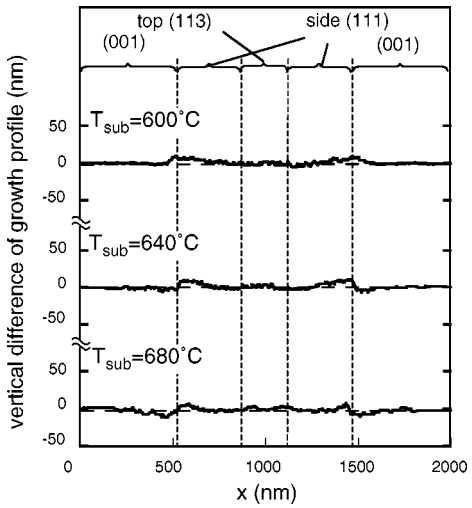

FIG. 9. Deviation of the calculated growth profile between from the experimental one.

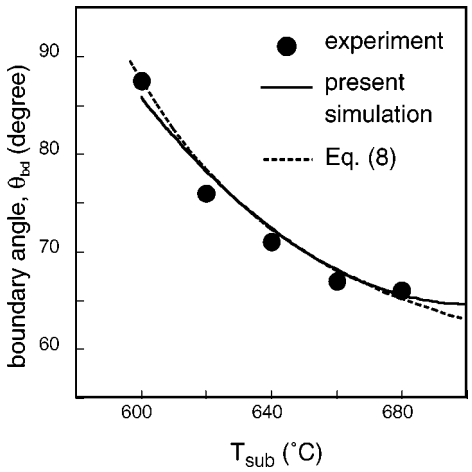

FIG. 10. Comparison of the value of the facet boundary planes, θ_{bd}, between the experiment and the present simulation.

around the boundary between the bottom (001) plane and the side (111) facets, as shown in Fig. 9. This may represent a limitation arising from the assumed simple piecewise linear functional form of $\tau(\theta)$ used in this study.

B. Evolution mechanism of facet boundary planes

Both the experiment and the simulation indicated that the facet boundary planes are formed in the AlGaAs ridge layers keeping the constant angle, θ_{bd}, throughout the entire growth. From the simple geometrical consideration, the boundary angle, θ_{bd}, should satisfy the following relation, as derived first in Ref. 7:

$$\tan\theta_{bd}=\frac{\alpha\cdot\tan\theta_{\text{side}}-\tan\theta_{\text{top}}}{\alpha-1}. \tag{8}$$

Here, α is the growth rate ratio defined as $\alpha=r_{\text{top}}/r_{\text{side}}$, where r_{top} is the vertical growth rate on the top facet and r_{side} is that on the side facet. θ_{top} and θ_{side} are the angles of top facet and side facet with respect to a flat top of mesa, respectively. In the case of ⟨110⟩-oriented wires grown on (001) substrates, the value of $\theta_{\text{top}}=25.2$ and $\theta_{\text{side}}=54.7$ should be used as the angle of top (113) facet and side (111) facets, respectively.

Figure 10 compares the values of the facet boundary angle, θ_{bd}, among the experimental values, the values obtained by Eq. (8) and the result of the present growth simulation. Excellent agreements between experiment and theory are seen in Fig. 10, where the difference among them was smaller than 1.5°. Thus, formation of facet boundary planes is a consequence of the difference of growth rates between the neighboring ridge facets caused by incorporation and lateral diffusion of adatoms. These results indicate that the lateral width of present ridge QWRs can be kinetically controlled by the growth conditions and the supply thickness of AlGaAs layer prior the start of wire growth.

Finally, the reason why the facet boundary planes became visible after etching in the wire cross sections, as clearly seen in Fig. 1(b), can be explained as follows. This is due to a slight change in composition between regions grown on (113) facets and (111) facets. Figure 11 shows the profile of Al composition change of AlGaAs ridge layer calculated for different values of T_{sub}. As seen in Fig. 11, Al composition on top (113) facets is reduced due to the enhancement of migration of Ga adatoms from side (111) facets to top (113) facets at higher growth temperatures. This composition difference along the facet boundary planes became visible by stain etching, where the GaAs is selectively dissolved into the etchant.

V. CONCLUSION

In order to understand and precisely control selective MBE growth of GaAs ridge QWRs, detailed investigation of the growth kinetics were made experimentally and an attempt was made to establish a simple theoretical model that can reproduce the growth features quantitatively. Experiments were carried out on the growth of ⟨110⟩-oriented

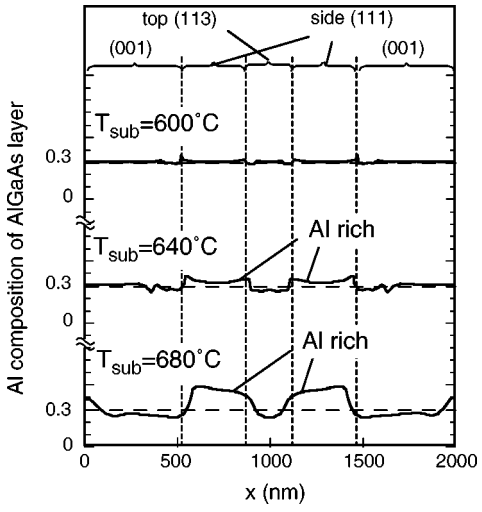

FIG. 11. Profiles of Al composition change in AlGaAs layers calculated for different T_{sub}.

AlGaAs–GaAs ridge quantum wires on mesa-patterned (001) GaAs substrates. A phenomenological modeling was made under the continuum approximation including macroscopic parameters such as group III adatom lifetime, diffusion constant and migration length. Computer simulation assuming a simple piecewise linear functional form for surface slope angle dependence of group III adatom lifetime reproduced the experimentally observed growth features such as the cross-sectional structure of the ridge wire and its temporal evolution, its temperature dependence and evolution of facet boundary planes.

The simple phenomenological modeling approach developed here seems to be of a general nature and may be very powerful for design and precise control of the crystal growth of nanostructures not only for the present ridge wire growth but also other varieties of structures.

ACKNOWLEDGMENTS

The work reported here is supported in part by 21st Century COE Project at Hokkaido University on ''Meme-Media Technology Approach to the R&D of Next-Generation Information Technologies,'' by Grant-in-Aid for Scientific Research (A)-13305020 and by Grant-in-Aid for Young Scientists (B)-14750223 all from the Japanese Government.

[1]E. Kapon, D. M. Hwang, and R. Bhat, Phys. Rev. Lett. **63**, 430 (1989).
[2]T. Fukui, S. Ando, Y. Tokura, and T. Toriyama, Appl. Phys. Lett. **58**, 2018 (1991).
[3]S. Koshiba, H. Noge, H. Akiyama, T. Inoshita, Y. Nakamura, A. Shimizu, Y. Nagamune, M. Tsuchiya, H. Kano, H. Sakaki, and K. Wada, Appl. Phys. Lett. **64**, 363 (1994).
[4]X. L. Wang, M. Ogura, and H. Matsuhata, Appl. Phys. Lett. **66**, 1506 (1995).
[5]H. Fujikura and H. Hasegawa, J. Electron. Mater. **25**, 619 (1996).
[6]T. Sato, I. Tamai, C. Jiang, and H. Hasegawa, Inst. Phys. Conf. Ser. **170-4**, 325 (2002).
[7]T. Sato, I. Tamai, and H. Hasegawa, Inst. Phys. Conf. Ser. **174-3**, 145 (2003).
[8]I. Tamai, S. Yoshida, T. Sato, and H. Hasegawa, Physica E (Amsterdam) **21**, 521 (2004).
[9]T. Takebe, M. Fujii, T. Yamamoto, K. Fujita, and T. Watanabe, J. Appl. Phys. **81**, 7273 (1997).
[10]G. H. Gilmer and P. Bennema, J. Appl. Phys. **43**, 1347 (1972).
[11]S. B. Ogal and A. Madhukar, Appl. Phys. Lett. **60**, 2095 (1992).
[12]A. K. M.-Beaghton and D. D. Vvedensky, Phys. Rev. B **42**, 5544 (1990).
[13]Y. Kangawa, T. Ito, A. Taguchi, K. Shiraishi, T. Irisawa, and T. Ohachi, Appl. Surf. Sci. **190**, 517 (2002).
[14]M. Ohtsuka and S. Miyazawa, J. Appl. Phys. **64**, 3522 (1988).
[15]M. Ohtsuka, J. Cryst. Growth **205**, 112 (1999).
[16]M. Ozdemir and A. Zangwill, J. Vac. Sci. Technol. A **10**, 684 (1992).
[17]P. S. Dominguez and F. Briones, Microelectron. J. **26**, 751 (1995).
[18]G. Biasiol, A. Gustafsson, K. Leifer, and E. Kapon, Phys. Rev. B **65**, 205306 (2002).
[19]T. Sato, I. Tamai, S. Yoshida, and H. Hasegawa, presented at ICFSI-9, 15–19 September 2003, Madrid, Appl. Surf. Sci. (to be published).
[20]M. Hata, T. Isu, A. Watanabe, and Y. Katayama, J. Vac. Sci. Technol. B **8**, 692 (1990).
[21]M. Hata, A. Watanabe, and T. Isu, J. Cryst. Growth **111**, 83 (1991).
[22]S. Koshiba, Y. Nakamura, M. Tsuchiya, H. Noge, H. Kano, Y. Nagamune, T. Noda, and H. Sakaki, J. Appl. Phys. **76**, 4138 (1994).
[23]J. M. Van Hove and P. I. Cohen, J. Cryst. Growth **81**, 13 (1987).
[24]K. Ohta, T. Kojima, and T. Nakagawa, J. Cryst. Growth **95**, 71 (1989).
[25]X. Q. Shen, D. Kishimoto, and T. Nishinaga, Jpn. J. Appl. Phys. **33**, 11 (1994).
[26]J. Gebauer, M. Lausmann, F. Redmann, R. Krause-Rehberg, H. S. Leipner, E. R. Weber, and Ph. Ebert, Phys. Rev. B **67**, 235207 (2003).